"Infrared Neurostimulation in Ex-vivo Rat Sciatic Nerve using 1470 nm Wavelength"

J. Cury[1,2], L. Vande Perre[1], H. Smets[1], L. Stumpp[3], S. Vespa[3], A. Vanhoestenberghe[4], P. Doguet[5], J. Delbeke[3], R. El Tahry[3], SP. Gorza[2] and A. Nonclercq[1]

[1] Bio, Electro and Mechanical Systems (BEAMS), Université libre de Bruxelles, Brussels, Belgium.
[2] Opera Photonics, Université libre de Bruxelles, Brussels, Belgium.
[3] Institute of Neurosciences (IONS), Université Catholique de Louvain, Belgium – Cliniques Universitaires Saint Luc, Department of Neurology, Brussels, Belgium
[4] Aspire Centre for Rehabilitation Engineering and Assistive Technology, University College London, UK.
[5] Synergia Medical, Mont-Saint-Guibert, Belgium.

E-mail: joaquin.cury@ulb.ac.be

Received xxxxxx
Accepted for publication xxxxxx
Published xxxxxx

Abstract

Objective: To design and implement a setup for ex-vivo optical stimulation for exploring the effect of several key parameters (optical power and pulse duration), activation features (threshold, spatial selectivity) and recovery characteristics (repeated stimuli) in peripheral nerves. *Approach:* A nerve chamber allowing ex-vivo electrical and optical stimulation was designed and built. A 1470 nm light source was chosen to stimulate the nerve. A photodiode module was implemented for synchronization of the electrical and optical channels. *Main results*: Compound Neural Action Potentials (CNAPs) were successfully generated with infrared light pulses of 200-2000 µs duration and power in the range of 3–10 W. These parameters determine a radiant exposure for stimulation in the range 1.59-4.78 J/cm^2. Recruitment curves were obtained by increasing durations at a constant power level. Neural activation threshold is reached at a mean radiant exposure of 3.16 ± 0.68 J/cm^2 and mean pulse energy of 3.79 ± 0.72 mJ. Repetition rates of 2–10 Hz have been explored. In 8 out of 10 sciatic nerves, repeated light stimuli induced a sensitization effect in that the CNAP amplitude progressively grows, representing an increasing number of recruited fibres. In 2 out of 10 sciatic nerves, CNAPs were composed of a succession of peaks corresponding to different conduction velocities. *Significance:* The reported sensitization effect could shed light on the mechanism underlying Infrared NeuroStimulation (INS). Our results suggest that, in sharp contrast with electrical stimuli, optical pulses could recruit slow fibres early on. This more physiological order of recruitment opens the perspective for specific neuromodulation of fibre population who remained poorly accessible until now. Short high-power light pulses at wavelengths below 1.5 µm offer interesting perspectives for neurostimulation.

Keywords — NIR neurostimulation, ex-vivo peripheral nerves, recruitment curve, optical single shots, sensitization effect, stimulation threshold, high spatial resolution.

I. INTRODUCTION

As a therapeutic tool, electrostimulation commonly involves activation or inhibition of excitable tissue by electrical current pulses delivered through electrodes [1-4]. The use of implanted stimulators started with cardiac pacemakers [5,6], now complemented with cardioverters and defibrillators [7,8]. Similar devices have been approved for a broad range of applications including deep brain stimulators for Parkinson's disease [9-11] and for various forms of tremors and dystonia [12,13]. At the limit between central and peripheral targets, we find cochlear and visual prosthesis [14,15]. The diaphragm or phrenic stimulators are used in respiratory paralysis [16,17]. Peripheral nerves are being stimulated for bladder incontinence [18,19], neuroprosthetic for foot drop [20,21], or walking aids [22,23]. Vagus nerve stimulation is an established treatment for refractory epilepsy and is currently being investigated for a broad spectrum of other conditions such as chronic pain [24-26], depression [27,28], obesity [29], migraine [30,31], heart failure [32] and gastroparesis [33,34]. However, electrical stimulation has major limitations such as: A) lack of spatial resolution due to the spreading of stimulating currents that are reaching neighbouring structures leading to unintended side effects such as muscle contraction or pain [35]; B) neural recordings are polluted by stimulation artefacts, prohibiting (CNAPs) recording in the vicinity of the stimulating electrodes [36,37]; C) neurostimulators are incompatible with Magnetic Resonance Imaging (MRI) because of device heating by induction and image distortion due to electromagnetic interference [38]; D) the order in which the nerve fibres are activated by electrical stimulation is almost opposite to the natural recruitment. Indeed, in physiological conditions, the smallest fibres are activated first while the largest fibres have the lowest threshold to electrical stimulation [39]. This is particularly important for

the vagus nerve, composed of a majority of small mostly non-myelinated fibres, hence difficult to stimulate electrically. Optical stimulation, inducing neural response to transient light pulses, could overcome most of these limitations [35-38,40-62]. This approach includes optogenetics, photoactive molecules and infrared neural stimulation (INS). In this study, INS is particularly emphasised, due to the potential for direct activation of neural tissue by infrared light, as opposed to techniques that rely on the introduction of exogenous light responsive molecules [63].

The biophysical mechanism underlying INS has been investigated by Wells et al., who concluded that photonic neural activation is a photothermal effect whereby a transient tissue heating activates the axon membrane [42]. Several hypothetical mechanisms have been proposed at the level of the cell membrane, including alteration of channel gating [42], thermosensitive ion channels (TRPV1 and TRPV4) [64,65,66], and membrane capacitance change [67]. Additionally, there is evidence supporting that INS destabilize the plasma membrane causing the formation of short-lived nanopores. This membrane nanoporation allows the influx of extracellular ions leading to neural activation [68]. While all these mechanisms are governed by local temperature variation, we should also point out the fact that light sensitive channels exist in nature (e.g., retina [69]) and that similar direct light effect might also be possible.

Studies have logically focused on the infrared part of the light spectrum due to the absorption peaks in water (considered as the main chromophore responsible for absorbing infrared light [42,67]). The range 980-2100 nm in particular has been shown to evoke a motor response when applied to the surface of a peripheral nerve, offering an optimum penetration depth matching the thickness of the nerve fiber. In the prospect of miniaturized applications, encouraging results have been obtained with wavelengths below 1500 nm. In this spectral range, 1470 nm waves may be promising because of an absorption peak in water similar to that of longer wavelengths (absorption coefficient ~ 30 cm^{-1} [70]). However, as the nerve is a turbid media, scattering also plays a role in light distribution by decreasing the optical penetration depth. Considering the water absorption coefficient and the reduced scattering coefficient measured in brain (~2 cm^{-1} [71-74]), as an approximation of this coefficient in sciatic nerve, the penetration depth at 1470 nm is estimated ~190 µm [75].

While most animals investigated in the literature are warm-blooded vertebrates selected for their physiological similarity to humans, there are other examples as well. In the context of INS, the studies can be classified in three main groups. A) In-vivo experiments in: humans [60], rats [36,43,44,48-50,53,55], gerbils [40,41,45-47,52,54] and quails [76]. B) Ex-vivo experiments in: rats [77], lobsters [37], aplysia [55], rabbits [78], bullfrog [79] and murine [80]. C) In-vitro experiments in: hippocampal and cortical neurons from rat [81,82], untransfected HEK-293T cells, X. laevis oocytes and artificial lipid bilayers [67]. This work focused on ex-vivo rather than in-vivo experimentation for several reasons. First, an ex-vivo setup provides a better control of parameters such as the surrounding temperature. Second, unwanted biological interactions such as stimulus triggered reflex activity are eliminated which simplifies the interpretation of results. Third, much better physical access to the preparation is possible and necessary if different exploration modalities are required (e.g., microscopy, electrical and/or optical stimulation). Fourth, the absence of anaesthetic drugs eliminates the potential interference with the nerve physiological state.

II. Materials and Methods

All experiments were conducted at the Institute of Neuroscience (IONS), Université Catholique de Louvain (UCL), Belgium, an animal care facility accredited by the Animal Care Service of the Federal Public Department. This work fully complies with a protocol approved (2019/UCL/MD/007) by the ethics committee for animal experimentation at UCL, in agreement with the ETS 123 European Convention.

A. Nerve Dissection and Preparation

22 Male Wistar rats 300 g ± 60 g obtained from the local breeding facility at the UCL were used. The animals were housed under a 12 h day/night cycle with controlled temperature and humidity, and ad libitum access to food and water. The anaesthesia was performed using Sevoflurane (6 %) in oxygen (1.5 lt/min). When the animal was under light sedation, an intraperitoneal injection of Ketamine (60 mg/kg body weight) and Xylazine (7 mg/kg body weight) was administered. Anaesthesia was maintained by boosting injections of Ketamine (60 mg/kg body weight) until the animal was sacrificed. Depth of anaesthesia was checked by the withdrawal reflex to noxious paw stimulation every 10 minutes. The surgery began with a skin incision on the lateral side of the hind limb from the knee to the hip region. The sciatic nerve (SN) was exposed after blunt dissection between the gluteus superficialis and biceps femoris muscles. To prevent drying during the surgery, the SN was regularly wetted with Hepes-buffered oxygenated Krebs Ringer solution (140 mm NaCl, 5 mm KCl, 2 mm $CaCl_2$, 1 mm $MgCl_2$, 5.5 mm HEPES, 11 mm D-glucose, pH 7.3, Fisher Scientific, Belgium) at room temperature. After the nerve had been carefully dissected free of surrounding tissue, a piece of suture thread was tied around it as close as possible to the knee joint at one end and near the spinal column at the other end. Then the nerve was cut free beyond the sutures leaving a 25-30 mm long nerve segment tied on each extremity. The ties avoid cytoplasm leakages and allow to gently handle the nerve by holding both suture threads. Thereafter, the nerve was placed into a 50 ml plastic tube with oxygenated Krebs-Ringer solution at room temperature for 20 minutes. The solution was gassed with pure oxygen (3 lt/min) for 120 minutes at room temperature during nerve dissection, so that the nerve could recover before CNAPs recordings.

B. Setup Overview

The schematic representation of the setup (Figure 1) to record CNAPs during electrical and optical stimulation includes: a nerve chamber, an optical stimulator, an electrical stimulator (for control purpose), the recording channel, a photodiode channel used for synchronisation, and a temperature sensor (Data acquisition 34970A, Keysight Technologies, USA). The output of the electrical recording channel was digitised at 200

kHz using a DAQ (6212 USB - 16 bits, National Instrument Corp., USA) and processed using MATLAB R2018 (MathWorks, Natick, USA).

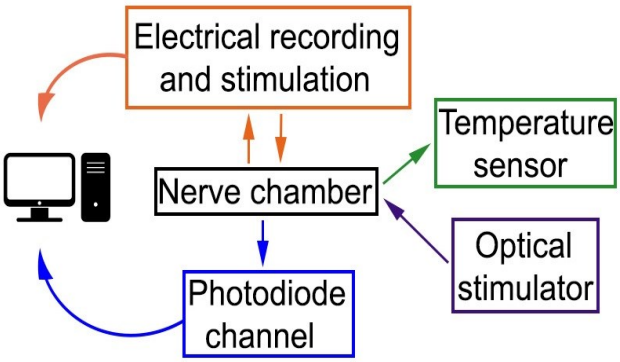

Figure 1. Schematic representation of the setup to record electrically CNAPs during electrical and optical stimulation.

C. *Nerve Chamber*

The nerve chamber (NC) was designed in Solidworks 2018 (Solidworks Corp., USA) and built from a photopolymer resin (Vero) by a 3D printer (Objet Eden260VS, Stratasys). The NC can hold the nerve, the electrodes and the optical fibre. The design is presented in Figure 2(A). The channel (a) is used to host the nerve, the vertical channel (b) to place the optical fibre for stimulation, and the diagonal channel (c) for housing the photodiode needed to detect the stimulation pulses (see section IIG). The photodiode is positioned at 4 cm from the sample and at an angle of 30° with respect to the optical fibre. Grooves made to host the electrodes (d) are separated by 1.4 mm (centre-to-centre).

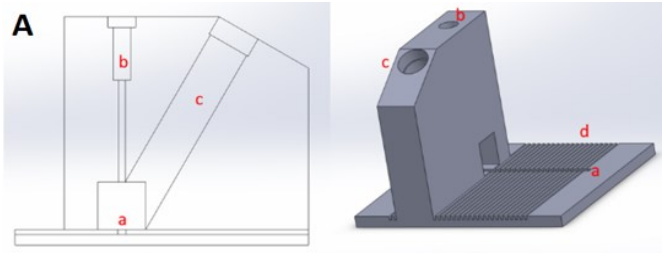

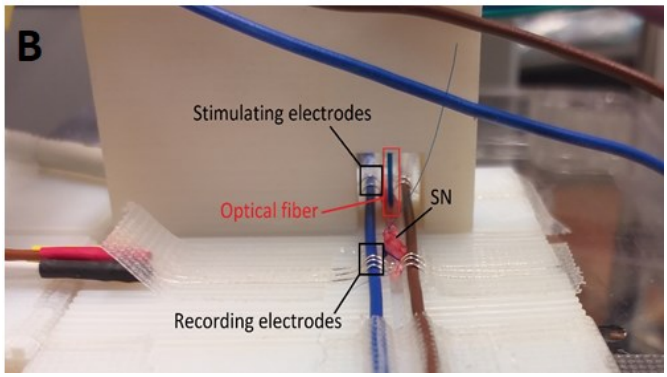

Figure 2. A: Diagram of the nerve camber. a) Hole to host the nerve. b) Optical fibre holder. c) Hole to host the photodiode. d) Grooves to host the electrodes. **B:** Picture of the chamber with the nerve, the stimulating and recording electrodes and the stimulating optical fibre. The blue and brown wires help to shape the electrodes.

D. *Electrical Stimulation and Recording*

The (custom-made) electrophysiological system is composed of a current-controlled stimulator and one amplifier. The stimulator generates biphasic square current pulses (negative pulse of 0.2 ms, then a zero-current pulse of 10 µs and finally a recovery pulse of 0.2 ms with opposite amplitude) ranging from 10 to 500 µA. In the recording channel, the amplifier includes a preamplifier (gain: 100), an amplifier (gain: 26), an isolation stage (gain: 0.3) and a filtering stage (1st order filter), with a 10-8000 Hz bandwidth. The overall resolution of this channel is 0.20 µV with a dynamic range of ± 3.46 mV, both referred to the input. The observed root mean square noise is 0.43 µV also referred to the input.

E. *Electrodes Disposition*

Five electrodes (99.99% silver wire, diameter 250 µm, Sigma Aldrich, Belgium) are used: two of them for stimulation [anode (1) and cathode (2)] and three of them for recording [GND (3), CNAP+ (4) and CNAP- (5)]. To minimise the stimulation artefact, the stimulating and recording electrodes are separated by the ground electrode (GND), used as a shield (Figure 3). The distance between the stimulating and recording electrodes (2 and 4) is 21.4 mm. The distance between the optical fibre (green dot) and the recording electrode (4) is 15.4 mm. Before the experimentation, the electrodes were cleaned several times with ethanol 70 % and rinsed with distilled water.

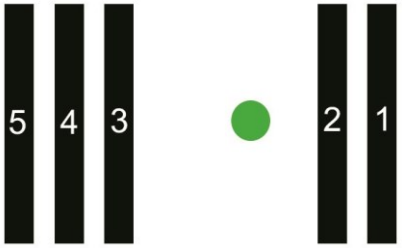

Figure 3. Diagram of the distribution of the stimulating (1,2) and recording electrodes (3,4,5) in the nerve chamber. 1: Anode. 2: Cathode. 3: GND. 4: CNAP+. 5: CNAP-.

F. *Optical Stimulator*

The optical stimulator is a NeoV 1470 nm (NeoLaser) originally developed for endovascular applications. The stimulation pulses were delivered to the sample by a multimode fibre (numerical aperture 0.22, core diameter 400 µm, Neo Laser), positioned perpendicular on top of the sciatic nerve and in contact with it. The power and duration of the optical stimulation monophasic square pulses can vary between 1–10 W (steps of 0.1 W) and 100 µs–30 ms (steps of 100 µs, except 300 µs), respectively. The optical stimulator can provide stimulation rates in the range of 0–50 Hz. A predefined sequence of identical pulses was triggered using a pedal switch connected to the laser driver. Before each experiment, the power at the output of the stimulating fiber is measured using a powermeter (13PM001, Melles Griot, Germany). Then, the optic fiber is placed within the nerve chamber to start the recordings. Note that in the results section, we always report the peak power delivered to the sample (measured with the powermeter). The power and pulse width used during optical stimulation, determines an energy/pulse in the range of 1-6 mJ.

G. Synchronisation Module

The precise timing of each stimulation pulse was recorded using a synchronisation module. This module is based on a photodiode (FGA10, InGaAs, 10 ns rise time, 900-1700 nm, Ø1 mm active area, ThorLabs) that detects individual optical stimulation pulse. It is connected to a passive circuit with a bandwidth of 430 kHz and generates a voltage signal proportional to the incident optical power. A real time threshold detection algorithm recovers the synchronisation timing for each laser stimulation of the nerve.

H. Computation of the Deposited Energy

In the literature about INS, the amplitude of the optical excitation, as well as the activation and damage thresholds are usually reported in terms of the radiant exposure (J/cm^2) [36,38,44,45,61]. However, as the underlying mechanisms leading to neural tissue stimulation is still poorly understood, we also report the pulse energy (mJ) as in [58]. The radiant exposure was calculated from the measured power and assuming a spot size diameter identical to the core fibre diameter (400 µm). This estimation is supported by the fact that the multimode optical fibre is in contact with the nerve.

I. Data Processing

Potential CNAP were first identified in the average of the unfiltered data (48-100 samples) over the full sequence. A CNAP was considered as potentially genuine when the filtered wave amplitude reached twice the background level (signal to noise ratio (SNR) ≥ 2). Confirmation was obtained by the comparison between the separate averages of odd and even samples of unfiltered data.

The validation phase of the set-up revealed that electromagnetic interferences from the environment, picked up by the recording electrodes and the electronic circuit, adds a non-negligible periodic background on the signal. This prevents small CNAPs to be accurately measured. In order to reduce these interferences, different procedures were performed. The noise sources in the set-up (circuits and cables) were shielded. The laser source was placed at 2 m (i.e., the maximum possible distance) from the set-up and all circuits were battery powered. However, even with these measures, the measurements still suffered from external perturbations. Because of this and the variability among recordings, we resorted successfully to a common digital imaging technique used for periodic noise reduction [83]. This technique could be of interest for research groups facing the same issue of large periodic background from external interferences.

As an example, a typical signal is shown in Figure 4(A). It can be seen that the CNAP, corresponding to the peak around 2.5 ms, has an amplitude comparable with the background fluctuations. This background signal could in principle be numerically filtered in the one-dimensional signal V(t), recorded for the full-stimulation sequence, with several notch filters located at the harmonics of its fundamental frequency. However, the background signal (which varies between the experiments), the periodic stimulation as well as the shape and duration of the CNAP, make this procedure difficult. The CNAP can, however, be more easily seen in its 2D map representation $g(\tau = t - nT, n) = V(t)$ for $(n-1)T \leq t < nT$, where T is the time duration between two stimulation pulses and n is an integer that corresponds to the order of the pulse in the sequence (see Figure 4(B)). In this two-dimensional map, the signal in each row is synchronised with the stimulation pulse. The CNAP is thus expected to be aligned with the vertical axis (see the vertical dark blue band around 2.5 ms in Figure 4(B)) and should thus be considered as the delay to the stimulation pulse. Conversely, the background appears as "tilted fringes" because of the difference between its fundamental frequency and the excitation frequency. In the two-dimensional Fourier transform of g(t, n), G(w,f), the spectral signature of the background can clearly be identified as peaks located at $f \neq 0$. In our example, the peaks at $f_{1\pm} \approx \pm 0.95$, $f_{2\pm} \approx \pm 1.9$, and $f_{3\pm} \approx \pm 5.72$, seen as horizontal bands in $|G|$ plotted in decibel scale, carry most of the background signal (see Figure 4(C)). These peaks are filtered with super-Gaussian notch filters of the form $1 - \exp\left[-\{(f - f_0)/\Delta f\}^{-6}\right]$ to remove the background (see Figure 4(F)). A low-pass super-Gaussian filter is also applied to remove frequencies higher than |f| = 5 as they do not significantly contribute to the CNAP. Figure 4(E) shows the two-dimensional map of the signal after this filtering procedure.

The filtered signal V(t) corresponding to the trace in Figure 4(A) is plotted in 4(D). We can see that the amplitude of the background has been reduced without significantly affecting the CNAP, revealing for instance the recovery period. Moreover, while the CNAP was very difficult to identify in the unfiltered data, it is clearly visible in the filtered signal (Figure 4(D)). Due to the variability of the environmental perturbations and the amplitude of the noise with respect to the CNAP, the position and the width of the notch filters and the cut-off frequency of the low-pass filter were adapted to filter the signal as best as possible without blurring it too much (as reported in corresponding Result sections). For very small CNAPs, the SNR was further enhanced by taking the average of the filtered signal over several stimulation pulses. The amplitude of the CNAPs was measured by subtracting in the filtered data, the peak value and the mean base line 5 ms before the electrical (optical) stimulus onset. The conduction velocity was calculated by dividing the distance from the optical fibre (or cathode) to electrode 4; and the latencies measured between the stimulus synchronisation pulse and the CNAP onset.

J. Stimulation Protocol

After nerve dissection and recovery in the solution, the sciatic nerve was placed in the nerve chamber with the optical fibre and the electrodes in contact with its surface. The temperature sensor was located 1 mm away from the optical stimulation site within the bathing fluid (Krebs Ringer). To maintain the sample hydration, drops of oxygenated Krebs Ringer solution at room temperature was applied on the SN using a syringe. First, a set of 2 biphasic current pulses at each amplitude level in the range 10–500 µA was applied to obtain an electrical recruitment curve and verify the state of the nerve. Optical stimulation settings in terms of number of pulses, power, pulse duration or stimulation

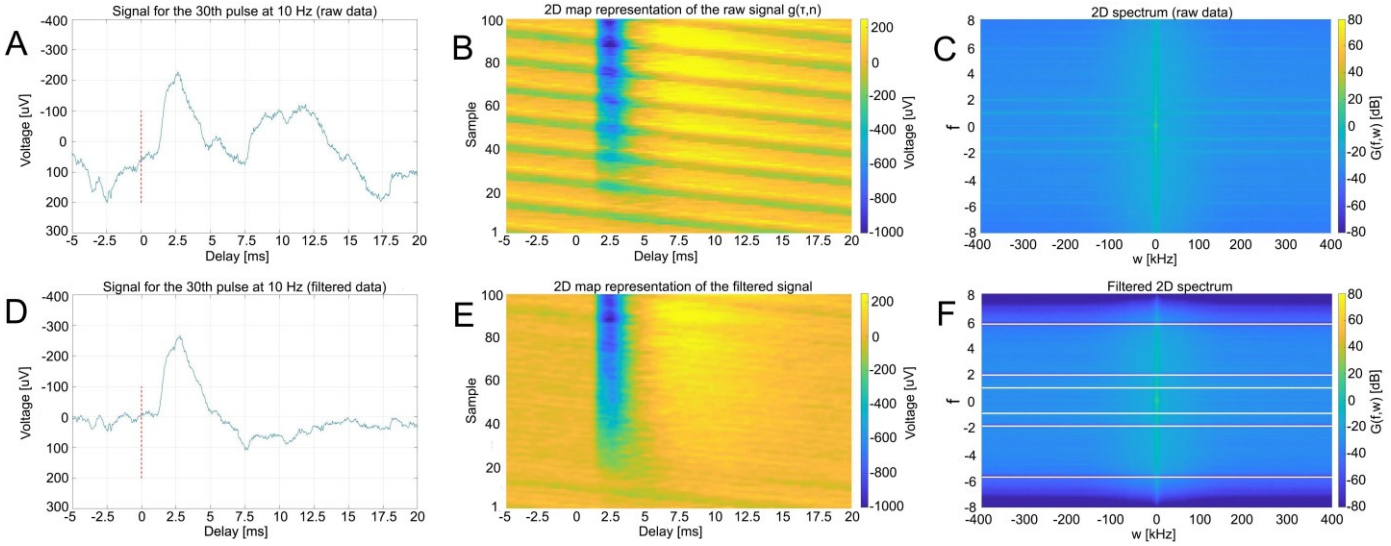

Figure 4. A: Measurement of the CNAP V(t) for the 30th stimulation pulse in a sequence taken at 10 Hz (raw signal, n = 30). **B**: 2D map representation of the raw signal g(τ,n). See main text for further explanations. **C**: Modulus of the 2D Fourier transform of g(τ,n) plotted in dB scale for clarity. **D**: Same signal as in (**A**) after the 2D filtering. Filtered 2D map (**E**) and spectrum (**F**). In this example 6 notch filters located at f = ± 0.95, ± 1.90 and ± 5.72 were used to remove the background fluctuations (white colour codes signal lower than -80 dB) and a low pass filter (cut-off |f|=5) further reduces the noise.

rate were adapted for the needs of each experiment and detailed in each corresponding results subsection. Trains of optical pulses instead of individual pulses were used with the intention to look at individual responses as a function of their rank in the train. In addition, these trains were also, useful to improve the signal-to-noise ratio through averaging. In all experiments, the power at the output of the fibre was measured before each recording and the temperature of the nerve measured before and after each train of optical stimulation pulses. Moreover, the nerve's responsiveness was tested after every set of two trains of optical stimulations by applying two electrical biphasic pulses of 300 µA and 0.2 ms/phase.

III. RESULTS

22 rats were used in this study. 12 of them were discarded, because of unsuccessful surgery or technical problems (five rats) or because response was obtained to electrical stimulation but no to optical stimulation (seven rats). In ten rats, CNAPs were recorded successfully on electrical and optical stimulations. Results from three rats, believed to be the most representative examples, are shown as illustration.

A. Stimulation Thresholds

The stimulation threshold for neural activation was explored by exciting the SN with trains of 48–100 optical pulses at 10 Hz with a power and duration starting at 10 W and 100 µs, respectively. These optical parameters determine a safe starting radiant exposure below 1 J/cm^2 [42,50,55,58]. This choice was motivated because short high-power pulses are more effective for stimulation [58] and short pulses better comply with thermal confinement regime [42,46].

The power was kept constant and the pulse duration increased in steps of 100 µs, until the threshold was reached. The power was then reduced in steps of 1 W and the pulse duration was increased by 100 µs, repeating the process until the threshold was obtained for all power/duration combinations. Three rats (RAT1-3) were used for this experimentation with the protocol described above. In addition, we report threshold values of RAT4-7 (used in other sections of this work), as a complementary information. The mean radiant exposure and energy required for neural activation are shown in Table 1. The values contributing the mean radiant exposure for each sample were plotted as a function of two stimulation parameters: peak power and pulse duration (see Figure 5).

TABLE 1: STIMULATION THRESHOLD

RAT	Mean radiant exposure [J/cm^2]	Mean energy [mJ]
1	3.31 ± 0.60	3.97 ± 0.71
2	3.84 ± 0.07	4.60 ± 0.08
3	2.83 ± 0.83	3.39 ± 1.0
4	3.36	4.03
5	3.33	3.99
6	2.45	2.94
7	3.20	3.84
Mean ± Std	**3.16 ± 0.68**	**3.79 ± 0.82**

The confinement of the laser energy in both space and time is critical for optical stimulation efficiency [46]. In the thermal confinement condition, the laser pulse is sufficiently short for the optically deposited energy to activate the nerve before the heat diffuses out of the optical area. The theory predicts that pulse durations must reach up to hundreds of milliseconds before breaking the confinement condition [84]. However, Izzo et al. showed in auditory neurons that heat diffusion starts being noticeable with pulse width greater than 300 µs [46]. Furthermore, Wells et al. obtained experimental evidence in rat sciatic nerve at 2120 nm, in which that heat diffusion starts to play a role on a shorter time scale, causing the efficiency of the CNAP generation to be considerably reduced for pulses longer than 10 ms [42]. In our study, the optical penetration is similar to [42], while the pulse duration in all the experiments is at least 5 times shorter. We can therefore assume to be in the

spatiotemporal thermal confinement condition. Based on the above considerations, the instantaneous temperature rise, just after a stimulation pulse, can be estimated by [46]:

$$T(z,0) = \frac{\mu a * H(Z)}{\rho * c} = \frac{\mu a * P * t}{\rho * c * A} \qquad (1)$$

where μa is the absorption coefficient of water at 1470 nm (30.6 cm^{-1} [70]), $H(Z)$ is the radiant exposure in function of the distance Z, $H(Z) = H(0) * e^{-Z/\delta}$, with δ the optical penetration depth (~190 μm), ρ is the density (1030 kg/m^3 for most soft tissues), c is the specific heat of the tissue with a value of 3600 J/kg°C, P is the power, t is the pulse duration and A is the optical beam area (0.12 mm^2). If we consider the mean radiant exposure required for reaching the threshold (3.16 ± 0.68 J/cm^2) to be equal at different power and duration combinations (i.e., confinement region), we can predict the instantaneous temperature rise at the nerve surface (26.1 ± 5.6 °C). If the averaged thickness of the epineurium and perineurium combined (~ 90 μm) is taken into account [85], the estimated temperature rise at the level of the first nerve fibres is 16 ± 3.5 °C. Being in a spatiotemporal confinement condition, we can expect a constant relationship between power and pulse duration to stress the aforementioned relation:

$$P * t = \frac{T * A * \rho * c}{\mu a} \qquad (2)$$

This equation (see dash line in Figure 5) is compatible with the general trend of experimental measurements reported in the Figure, though more experimentation is required, on a wider range, to validate this model.

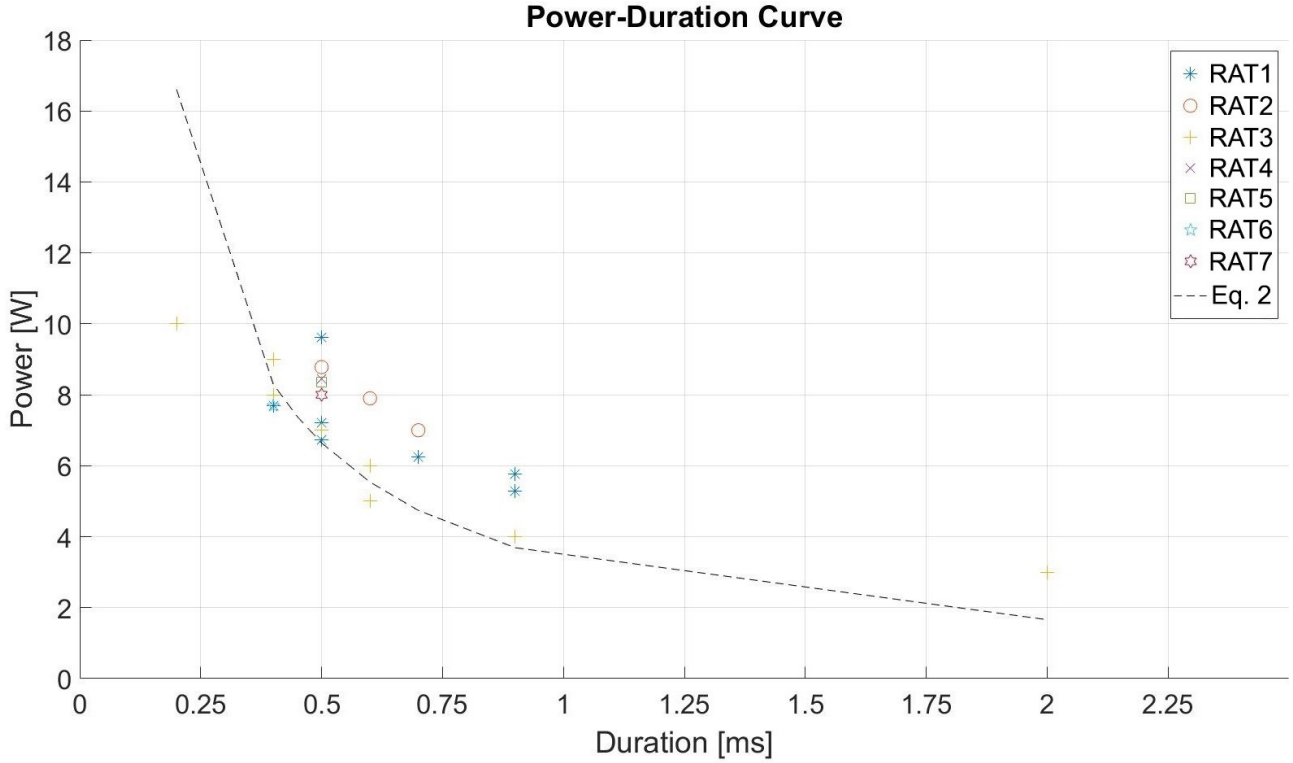

Figure 5. Peak power and pulse duration for neural activation in different samples (RAT1-7). The dash line represents the equation 2.

B. Optical Recruitment Curve

The optical recruitment curve of the SN was obtained by stimulating with trains of 48–110 optical pulses at 10 Hz with powers in the range 9–10 W and pulse durations starting at 100 μs up to 600 μs, with incremental steps of 100 μs. The stimulation was stopped when a CNAP was first noticeable (see section II.*J*) and without exceeding a radiant exposure of 5 J/cm^2. Figure 6(A) shows in RAT1 the response to a set of electrical pulses, with no filtering nor averaging. As expected, the CNAP does not appear at the lowest stimulation amplitude levels (below 20 μA), then becomes visible and reaches a plateau at the highest stimulation amplitudes (above 50 μA). Recorded CNAP amplitudes in all the experiments ranged from 16.4–3795 μV. Figure 6(B) shows the optical recruitment curve for the same rat at a fix power of 9.1 W and pulse width ranging from 100–400 μs for a stimulation rate of 10 Hz. As expected, the CNAP has a small amplitude at low stimulus duration (100 μs) and grows as the pulse width increases (200–400 μs). Recorded CNAP amplitudes ranged from 1–938 μV. It is important to notice that the electrical stimulation artefact is visible in Figure 6(A) while totally absent in Figure 6(B) despite the high gain.

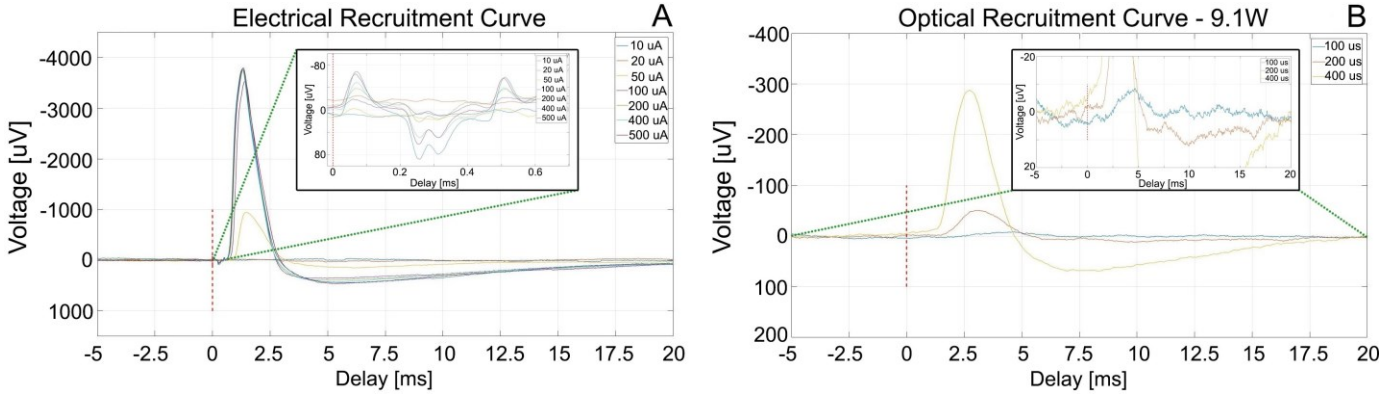

Figure 6. A: Electrical Recruitment Curve from RAT1. Raw data with no filtering and no averaging. The red dash line represents the electrical stimulus onset. The CNAPs amplitude ranged between 947–3795 µV. The inset shows the stimulation artefact. **B**: Optical Recruitment Curve at 9.1 W, average of 107 epochs at 10 Hz from RAT1. The radiant exposure ranged from 0.76–3.03 J/cm^2. The energy pulse ranged from 0.91–3.63 mJ. The red dash line represents optical stimulus onset. The signals are not filtered. The inset shows a small CNAP (≈ 9 µV) for a pulse duration of 100 µs. As the pulse width increases, the CNAP increases. With a pulse duration of 200 µs and 400 µs, the CNAP has an amplitude of ≈ 52 µV and ≈ 286 µV, respectively.

C. *Sensitization Effect*

We found evidence of a "*sensitization effect"*, in which the CNAPs amplitude (proportional to the number of activated fibres) becomes larger when the optical stimulation is preceded by other optical pulses. This phenomenon was observed in 8 rats, at different powers in the range of 7–10 W, for pulse durations from 200–700 µs and stimulation rates 4.16 Hz and 10 Hz. RAT1 and RAT10 believed to be most representatives are shown as illustration of this effect. In Figure 7, we show 3 types of graphs for each row: the 2D map of the raw data (left), the 2D map of the filtered data (middle) and train of optical pulses divided in 2 to 4 groups, filtered and averaged, to visualise the evolution of the signal amplitude (right). These approaches show an increasing amplitude of the CNAP as the sequence of stimulation pulses rise. Furthermore, the stimulation rate has an impact on this trend, being higher at 10 Hz than at 4.16 Hz while at 2 Hz, we did not find evidence of sensitization. In addition, the temperature change ΔT (measured 1 mm apart from the optical fibre) increased differently based on the stimulation rate. For instance, in RAT10, we measured ΔT equals to 1.16 ± 0.16 °C at 10 Hz, 1 ± 0.2 °C at 4.16 Hz and 0.3 ± 0.2 °C at 2 Hz.

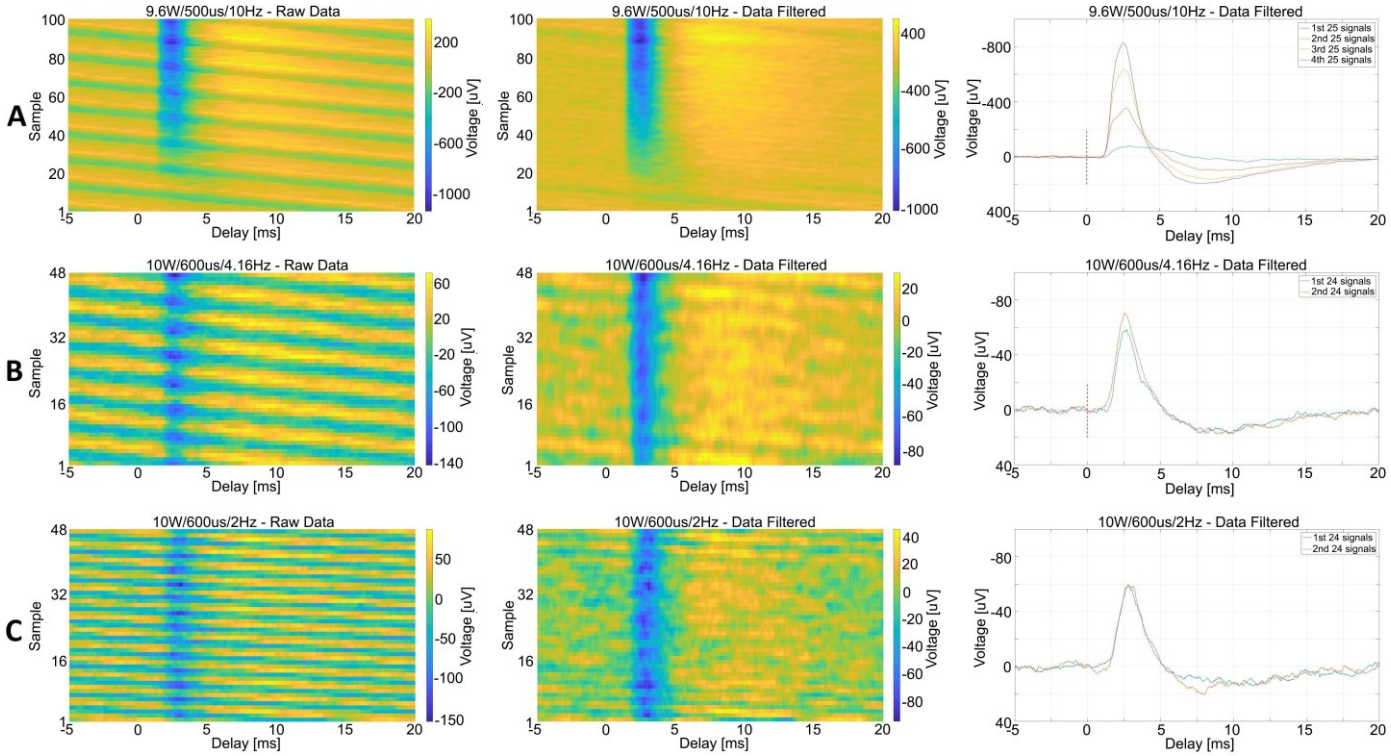

Figure 7. To investigate the amplitude of the CNAPs and its relationship with the number of pulses and the stimulation rates, trains of 50–100 optical pulses with a power from 9-10 W and a pulse duration in the range 500–600 µs were applied to the SN. For each train, different pulse rates were used (10 Hz, 4.16 Hz and 2 Hz). Each row displays the 2D map of the raw data (left), the 2D map of the filtered data (middle) and train of pulses divided in groups and averaged to compare the amplitude evolution of the CNAP (right). For instance, in (B), the 48 samples are divided in two groups, the former corresponding to the average of the signal

1-24 and the latter from 25-48. **A:** Sensitization effect observed in RAT1 for a sequence of 100 optical stimulation pulses at 9.6 W, 500 µs in a train at 10 Hz. The radiant exposure was 3.86 J/cm^2. The energy pulse was 4.63 mJ. 6 notch filters located at f = ± 0.95, ± 1.90 and ± 5.72 and a low-pass filter (cut-off |f|=5) were used. **B:** Sensitization effect observed in RAT10 for a sequence of 48 optical stimulation pulses at 10 W, 600 µs in a train at 4.16 Hz. For A and B, the radiant exposure was 4.78 J/cm^2 and the energy pulse was 5.73 mJ. 2 notch filters located at f = ± 2.01 and a low-pass filter (cut-off |f|=3) were used. **C:** Sequence of 48 optical stimulation pulses at 10 W, 600 µs in a train at 2 Hz (RAT10). The sensitization effect at 2 Hz is not present as using higher stimulation rates. 4 notch filters located at f = ± 3.77 and ± 5.66; and a low-pass filter (cut-off |f|=5) were used.

D. Optical Single Shot

CNAPs with SNR ≥ 2 after filtration were obtained in response to single optical pulse in the 10 rats at different powers in the range of 3–10 W with pulse duration from 200–2000 µs and rates (2 Hz, 4.16 Hz and 10 Hz). Figure 8 shows single pulse epochs CNAPs obtained in RAT10 at the beginning (4th) and at the end (40th) of each train of 48 pulses 10W/600µs at those 3 stimulation rates.

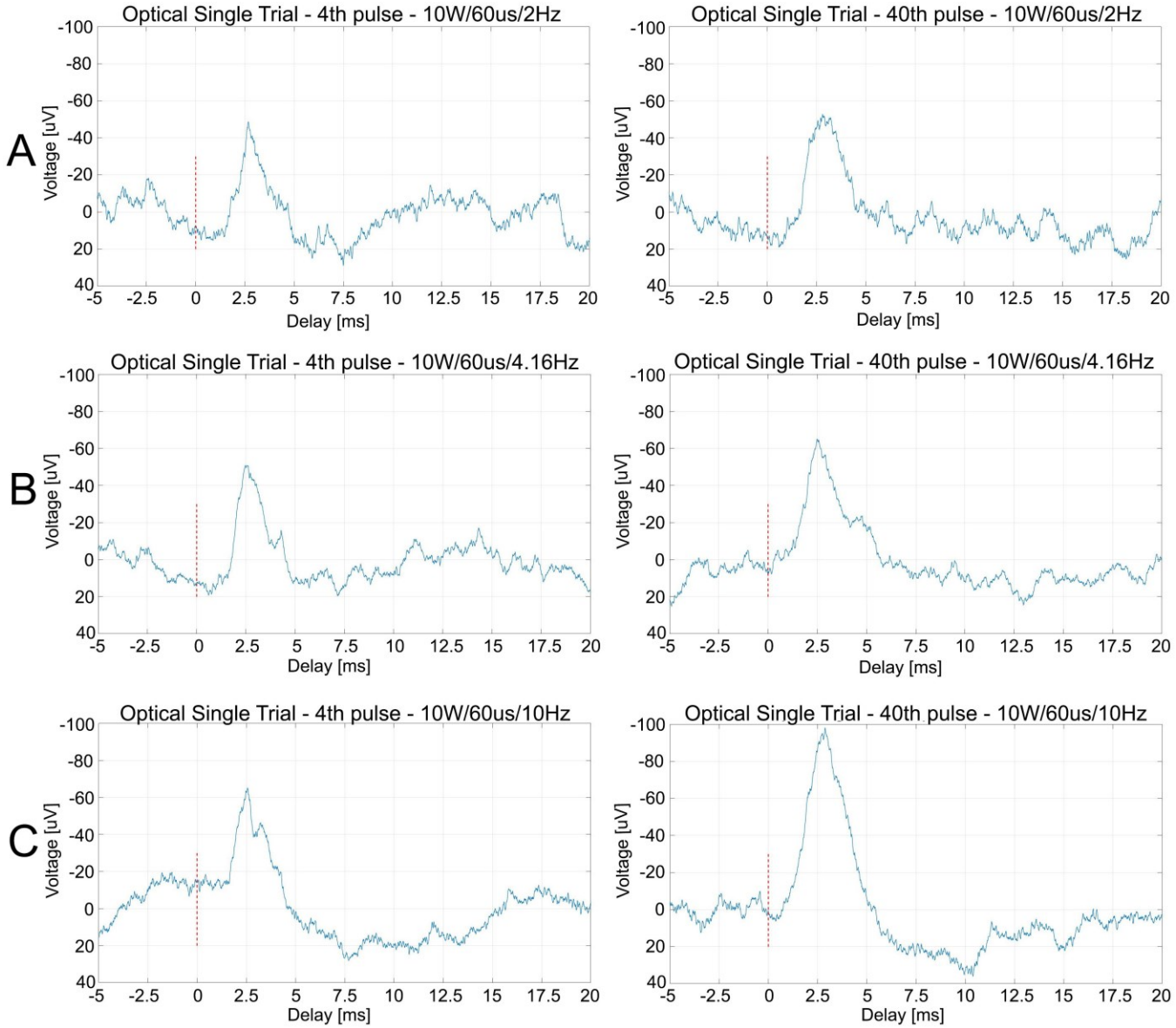

Figure 8. Optical single trials obtained from a train of optical stimulation pulses at fixed power and pulse duration with different excitation rates on RAT10. The radiant exposure was 4.78 J/cm^2. The energy pulse was 5.73 mJ. The red dashed line represents the optical stimulus onset. All signals are filtered as explained in the method section. The amplitude of the signal was calculated by taking the peak value of the CNAP and the mean baseline 5 ms before the optical stimulus onset. **A:** Optical single epoch at 10 W, 600 µs extracted from a 2 Hz train. 4 notch filters located at f = ± 3.77 and ± 5.66; and a low-pass filter (cut-off |f|=5) were used. Left: CNAP with an amplitude of ≈ 51 µV, in response to the 4th stimulation pulse. Right: CNAP with an amplitude of ≈ 55 µV, in response to the 40th stimulation pulse of the train. **B:** Optical single epoch at 10 W, 600 µs extracted from a 4.16 Hz train. 2 notch filters located at f = ± 2.01 and a low-pass filter (cut-off |f|=3) were used. Left: CNAP with an amplitude of ≈ 52 µV, in response to the 4th stimulation pulse. Right: CNAP with an amplitude of ≈ 75 µV, in response to the 40th stimulation pulse of the train. **C:** Optical single epoch at 10 W, 600 µs extracted from a 10 Hz train. 2 notch filters located at f = ± 1.16 and a low-pass filter (cut-off |f|=5) were used. Left: CNAP with an amplitude of ≈ 63 µV, in response to the 4th stimulation pulse. Right: CNAP with an amplitude of ≈ 99 µV, in response to the 40th stimulation pulse of the train.

E. High Spatial Resolution – Fibre Selection

Preliminary trials also pointed towards the high spatial resolution and fibre selectivity achievable with optical stimulation. In 8 rats, CNAPs were composed of a single peak. On the contrary, in 2 samples, we observed clear evidence of signals with different conduction velocities. It is important to highlight that CNAPs obtained in response to electrical and optical stimulations were acquired with the same recording electrodes, and are thus considered as originating from the same branch of the nerve (Figure 9). Yet, they differed in the nerve response and CNAP conduction velocities. Figure 10 shows results for RAT8. The electrically evoked CNAP reached an amplitude of 1317 µV and the estimated conduction velocity is 68 m/s. For the same rat, after optical stimulation, four successive peaks were distinguished with various amplitudes (**a:** 85 µV, **b:** 34 µV, **c:** 11 µV and **d:** 10 µV) and conduction velocities (**a**: 70 m/s, **b:** 4.7 m/s, **c**: 3 m/s and **d:** 2.3 m/s). In RAT7, a similar signal was observed for the electrically evoked CNAP. For the same rat, after optical stimulation, five successive peaks were distinguished with amplitudes (**a:** 60 µV, **b:** 56 µV, **c:** 30 µV, **d:** 19µV and **e:** 22 µV) and conduction velocities (**a**: 72 m/s, **b:** 5 m/s, **c**: 2.9 m/s, **d:** 2.2 m/s and **e:** 1.5 m/s).

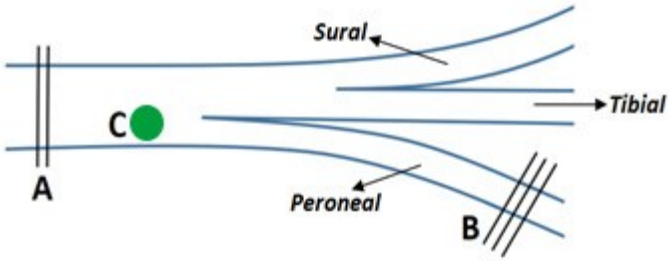

Figure 9. Representation of the rat sciatic nerve. For all the animals in this study, the electrical and optical stimulation were performed in the main trunk of the tibialis nerve and the recording was performed in one of the nerve branches (Peroneal). **A**: Stimulation electrodes. **B**: Recording electrodes. **C**: Optical stimulation.

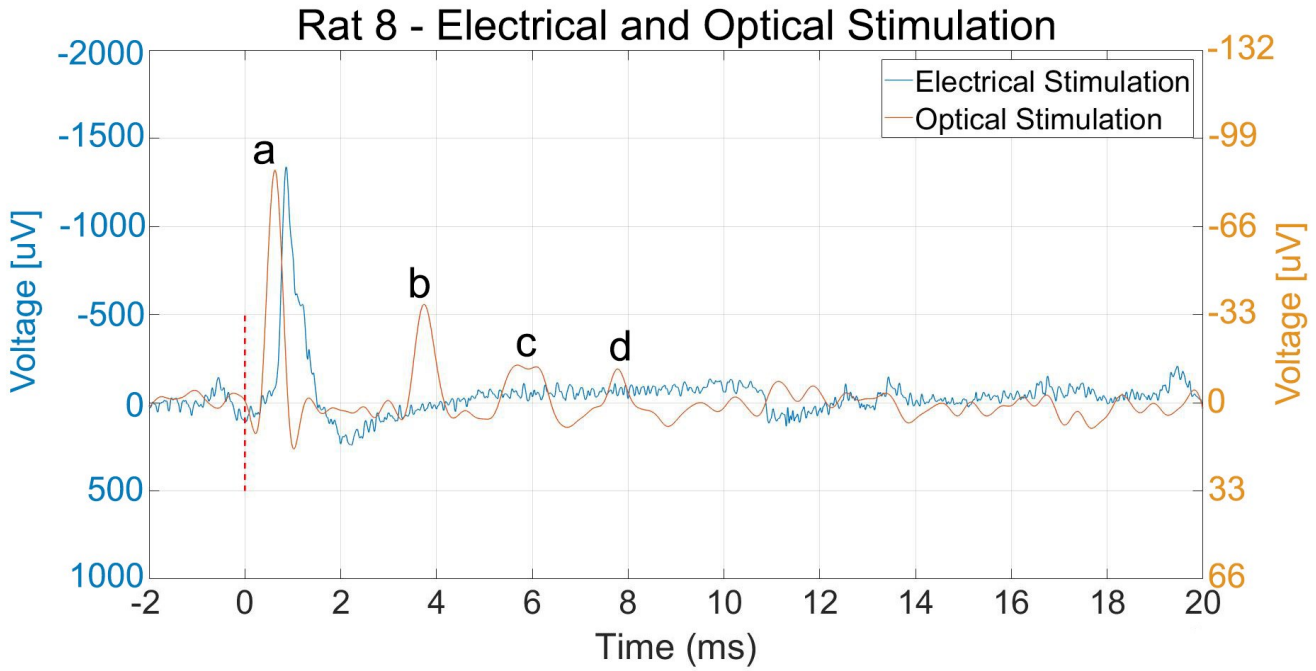

Figure 10. Electrical and Optical stimulation in RAT8. The red dash line represents the electrical (optical) stimulus onset. Due to the low amplitude of the slow CNAPs, signals were 2D filtered in the sample axis f and in the frequency axis w, and then averaged to improve the SNR (see Section II.*I*). The room temperature was 20°C for both experiments. **Blue**: Recording obtained after sending one electrical stimulation pulse with an amplitude of 50 µA and duration 0.2 ms in RAT8. **Orange:** Recording obtained after averaging 98 epoch signals of optical stimulation at 7.7 W, pulse duration 600 µs and 10 Hz in RAT8. The radiant exposure was 3.68 J/cm^2 and the pulse energy 4.41 mJ.

IV. Discussion

Electrical stimulation has been the gold standard for neuroprosthetics and neuromodulation devices [86]. However, this approach has shown limitations in therapeutic applications. For instance, the current spreading in tissue does not allow precise stimulation targeting, leading to a reduced resolution, in particular for spinal cord stimulators [87] as well as retinal and cochlear implants [88,89]. Even high contact density electrodes are restricted by the safety limit of high current density [90]. Penetrating electrodes are often not an alternative because of the traumatic nerve damage [91]. Additionally, non-myelinated C-fibers have a high threshold to electrical stimulation, thus remaining out of reach in most clinical neuromodulation applications such as in vagus nerve stimulation. Optical stimulation may overcome these drawbacks, by targeting small areas in the order of hundreds of micrometers without any tissue-electrode interface and probably characterized by a different fiber recruitment order.

In this study, we report CNAPs elicited by INS in ex-vivo rat sciatic nerve with a laser source operating at 1470 nm. This animal model was used due to the anatomical and physiological similarities with humans, having in mind a potential clinical application as well as a good candidate to be used in a laboratory facility. The radiant exposures for stimulation threshold obtained span from 2.48-3.84 J/cm^2. Table 2 shows the radiant exposure for stimulation threshold reported in literature for sciatic nerves at different wavelengths. To explain the large variability among wavelengths and with in-vivo vs. ex-vivo experiments, we suggest several hypotheses.

TABLE 2
INS THRESHOLD FOR RAT AND RABBIT SCIATIC NERVE ACTIVATION (THERMAL CONFINEMENT REGIME)

Reference	λ (nm)	Animal	Experiment	Beam size [mm^2]	Radiant exposure [J/cm^2]	Energy pulse [mJ]
Wells [44]	2120	Rat sciatic nerve	In-vivo	0.5 - 1	0.32 ± 1	1.6 ± 0.5 3.2 ± 1.0
Wells [43]	2120	Rat sciatic nerve	In-vivo	1.2	0.4	4.8
Duke [50]	1875	Rat sciatic nerve	In-vivo	0.36	1.7 ± 0.3	6.0 ± 1.1
Duke [56]	1875	Rat sciatic nerve	In-vivo	0.24	2.0 ± 0.4	4.9 ± 1
Duke [55]	2120	Rat sciatic nerve	In-vivo	0.12	1.12	1.34
McCaughey [51]	1495	Rat sciatic nerve	In-vivo	0.12	3.7 ± 2.8	4.4 ± 3.4
	2120		In-vivo	3.80	0.45 ± 0.05	19 ± 1.9
Peterson [58]	1875	Rabbit sciatic nerve	In-vivo	0.12	1.98	2.5
Throckmorton [62]	1450	Rat sciatic nerve	In-vivo	0.28	≈ 1	≈ 2.8
	1470					
	1875					
	2120				≈ 0.7	≈ 1.96
Dautrebande [38]	1470	Rat sciatic nerve	In-vivo	0.031	0.05-0.42	0.15-1.32
This study	1470	Rat sciatic nerve	Ex-vivo	0.12	3.16 ± 0.68	3.79 ± 0.82

First, from Table 2, considering the literature data about thresholds to stimulation with similar beam size, it can be stated that higher wavelengths require lower mean radiant exposures. For instance, the mean radiant exposure at 2120 nm is 1.12 J/cm^2, at 1875 nm is 1.98 J/cm^2, at 1495 nm is 3.7 J/cm^2 and at 1470 nm is 3.16 J/cm^2. To explain this difference, we hypothesise that another chromophore besides water, such as lipids (main constituent of the nerve membrane), could play a role in the efficiency of energy accumulation and confinement in INS. Table 3 summarises literature data about the absorption coefficient in fat at the wavelengths listed above. At 1870 nm and 2120 nm, the μ_{afat} is ≈ 14 and ≈ 142 times higher than at 1470 nm and 1490 nm. This could therefore at least partially explain, the decrease of energy threshold with longer wavelengths.

TABLE 3: ABSORPTION COEFFICIENT IN WATER AND FAT

λ (nm)	μa water (cm^{-1})			μa fat (cm^{-1})
	[92]	[93]	[94]	[95]
1470	30.60	24.82	28.61	0.14
1490	24.92	19.41	22.63	0.14
1870	28.85	22.63	34.82	2.00
2120	26.62	24.01	24.92	20.0

Second, while in-vivo studies using the same wavelength show similar radiant exposure for activation, comparing in-vivo (and usually through the motor response) with ex vivo (nerve response) leads, as expected, to a much large variability. In these studies, compound muscular action potentials (CMAPs) were recorded instead of CNAP. In this regard, CMAPs are at least one order of magnitude larger than CNAPs.

Furthermore, motor nerve fibers (large myelinated fibers about 10-12 μm diameter) are much easier to record from muscles. This may support the fact that Dautrebande et al. could not measure any CNAP while CMAP were successfully obtained during the recordings [38]. In line to this, Cargill et al. 2008 has also claimed dissimilarities between in-vivo and in-vitro experiments of murine sciatic nerve [80]. Third, Throckmorton et al., showed that radiant exposures to reach the threshold at 2120 nm were lower to those for diode laser at 1450 nm and 1470 nm, due to an initial microsecond high-power spike at the beginning of the excitation pulse in the Ho:YAG laser [62]. In this respect, we recommend to perform an analysis with different laser sources at different wavelength, with the same experimentation type (i.e., in vivo or ex vivo, motor or nerve response, etc.), to focus only on the impact of the wavelength and the pulse profile. Also, regarding Table 2, the energy requirements for neural activation during electrical and optical stimulation may differ due to the difference in the underlying mechanism for each approach. For instance, in our study, the energy required to evoke a CNAP electrically (~ 1-2 nJ) is much lower than the one required to evoke a CNAP optically (see Table 2). To compute this energy, we considered the current range to reach the threshold (20-50 μA), the stimulation and recovery pulse width (200μs+200μs) and the nerve impedance between the stimulating electrodes. The nerve impedance measured (0.77 kΩ/mm) was in agreement with the literature [96,97]. Electrical stimulation seems a more energy-efficient process, however, it is constrained by the low spatial resolution and relatively low allowable current density. Optical stimulation may overcome these limitations by depositing most of its energy in specific sections of the tissue.

We found evidence of a sensitization effect in INS, in which the number of activated fibres becomes larger when the optical stimulation pulse is being repeated. This phenomenon was observed at 4.16 Hz and 10 Hz. In some experiments a saturation effect was detected, in which the CNAPs amplitude did not increase after a given number of stimulation pulses (Figure 7(A)). Moreover, while at 10 Hz the increasing trend of the CNAPs amplitude was always noticeable, in some rats this effect was bigger than in others. For example, for the same stimulation rate, the sensitization is more important in RAT1 (Figure 7(A)) than in RAT10 (Figure 8(C)). For 2 Hz, we found no evidence of CNAPs amplitude dependence on the ranking order as seen in Figure 7(C). We believe this sensitization effect arises from the increase in temperature due to the energy deposition during stimulation. This increase was directly confirmed by monitoring the local temperature. In line to this, there is evidence of an increase in the force response of the plantarflexor muscle from rats, to both electrical and hybrid stimulation when the nerve has been preconditioned with an optical pulse [56]. This work suggested that optical stimulation increases the nerve's baseline temperature, thus enhancing the nerve's excitability to electrical stimulation in that region. At least four hypothetical mechanisms of sensitization linked to temperature can be proposed:

- Heat accumulation and diffusion could sensitise heat-activated channels (TRPM2 and TRPV1) of the nerve membrane [98], leading to a lower threshold and the recruitment of more fibres. In line with this proposal, Cesare et al. suggested that temperature rise causes heat-sensitive channels in neurons to change to a more disorganised and sensitive state [99].
- Peripheral sensitization, known as the increase in response of sensory nerve fibres (A-δ and C) and the decrease in the threshold to thermal, chemical and mechanical stimuli in the frame of tissue injury and inflammation [100]. Conditioning stimuli induce the release of potassium and a wide range of signalling molecules (ATP, prostaglandins, cytokines, protons and others) activating nociceptors and non-neuronal cells mediating the peripheral sensitization [101]. It has been claimed that radiant energy as low as 2 J/cm² could damage tissues [36,44], while in our work, the mean radiant exposure to reach neural activation threshold was 3.08 J/cm^2 (see Table 1 for further details).
- Heat accumulation and thermal diffusion could alter the voltage sensitive ion channels, leading to a change in their kinetics and therefore in the opening and closing rates of the voltage gates [42]. The degree of temperature dependence is quantified by the Q^{10} coefficient which describes the ratio between the rate of a biological process at two temperatures separated by 10°C [102]. Opening and closing rates of voltage sensitive channels present a typical Q^{10} value in the range 2–4. The conductance increase (ionic diffusion) due to temperature shows a Q^{10} value in the range 1.2–1.4 [103]. This is well described by the Hodgkin-Huxley model where the threshold for activation decreases due to the change in kinetics of the voltage gates.
- Shapiro et al. obtained experimental evidence showing that infrared-induced currents are produced by a transient change in the membrane electrical capacitance after local heating [67]. Heat accumulation could produce a decrease in the membrane capacitance and therefore an increase of the voltage threshold for nerve activation.

The temperature rising in the nerve based on the excitation rate is supported by [42], in which stimulation rates less than 5 Hz are recommended to avoid heat accumulation. Our results in Figure 7(C) shows that the sensitization effect is not present at 2 Hz in agreement with a lower heat accumulation in the optical zone at low rates. Therefore, we suggest that the sensitization effect results from a local increasing in temperature.

Following the assumption that neural activation takes place before heat starts to dissipate significantly [42,46], the temperature reached at the level of the nerve fibres is expected to be proportional to the deposited energy, in agreement with [46]. However, in several multidisciplinary fields such as INS, optogenetics and optochemistry, the metric for describing neural activation and damage threshold, is the radiant exposure (J/cm^2). This is understandable since the spot size distributing the energy over different volumes could suggest the use of density (radiant exposure) as the main parameter. However, for a nerve fibre, point activation of a single node of Ranvier or the simultaneous activation of a whole range of nodes will produce the same all-or-nothing action potential. These discrepancies are reflected in Table 2, summarizing the experimental studies of INS performed in sciatic nerves in warm-blood animals. To the best of our knowledge, 2 studies analyzed the relationship between the spot size diameter and the radiant exposure

threshold (or the energy threshold). The first work provides experimental data in rat sciatic nerve, suggesting that for any given wavelength, the spot size does not have an effect on the stimulation threshold [62]. The second work, modeled the nerve activity under INS, indicating that for a fixed energy and fiber-tissue distance, the temperature variation is higher for smaller spot size [104].

An important consideration for long-term applications of INS is the heat build-up. While heat accumulation over time may potentially damage the tissue, nerve exposition to relatively high temperatures can be tolerated for short amount of time. For instance, mammalian cells can survive to temperatures up to 42–47 °C for several seconds, while higher temperatures can only be tolerated for a limited duration [105]. Increasing the temperature has several effects on the nerve, including lowering the stimulation threshold, increasing the conduction velocity and potentially damaging the tissue. Optical stimulation parameters such as energy density, pulse duration, excitation rate, wavelength determining the penetration and absorption depth, and thermal relaxation time have a direct impact on the increase of temperature and the duration the nerve is exposed to it. In our experiments, the nerve's base temperature was 20°C, yielding an estimate average peak value of 46°C, in line with other temperature rises reported in the literature [82]. While this range seems relatively high, the pulse duration is short (i.e., shorter than 2 ms) and so is the thermal relaxation time in the nerve (around 90 ms as reported in [42]). Even if we do not know precisely how long the nerve is exposed to the high temperature, the pulse duration and thermal relaxation are orders of magnitude below known damaging exposure times. This is in keeping with our observation of maintained nerve functionality for the whole duration of the experiment, while regularly assessing its healthiness through regular evoked electrical stimulations.

Wells et al. recommended stimulation rates below 5 Hz to avoid thermal build-up [42]. Nevertheless, we suggest that a short train of optical pulses with a repetition rate higher than 2 Hz may be tolerated if compensated by a shorter train duration. In this regard, alternative means to limit heat exposure during INS, can be suggested. For instance, adequate focusing of the light beam on the functional target can save energy delivery and hence heat production. Additionally, we found that a lower radiant exposure was required for neural activation with shorter pulses (even if this corresponds to a stimulation power increase). As an illustration, with a pulse width of 200 µs, 10 W is required evoke a CNAP, leading to a radiant exposure of only 1.59 J/cm^2. Whereas, with a pulse width of 2 ms (i.e., much longer), 3 W is still required evoke a CNAP, leading to a radiant exposure of 4.78 J/cm^2, i.e., much larger. As a result, we recommend a shorter high-power pulse, for a more effective stimulation as suggested by Peterson et al. [58] and also, a short pulse will better comply with the thermal confinement regime [42,46]. Furthermore, the energy density to reach the threshold can be reduced if a subthreshold electrical stimulus is applied before INS. This preconditioning of the nerve will require lower optical energy for stimulation [50,56]. In agreement with [56], the sensitization effect observed in our study could precondition the nerve, i.e., decreasing the fiber threshold of both electrical and hybrid stimulation. If confirmed, optical pulses could for instance lower the electrical threshold of unmyelinated fiber (C-fibers), otherwise difficult to activate.

Strength-duration curves, similar to the optical power/duration relationship reported in this work, are commonly used to characterise the neural electrical stimulation. Different models have been proposed in the literature to describe the electrical current needed to reach the nerve activation threshold at a given pulse duration: the Weiss–Lapicque hyperbolic equation [106] and the Lapicque–Blair exponential equation [107]. We know that while these two approaches essentially describe the electrical charging of the cell membrane capacitance [108], the same mechanism is, of course, not at stake with optical stimulation. In this case, we conjecture that a constant transient temperature change is the main factor characterising what has now become the power-duration relationship. For this proposed model, heat diffusion is not considered as a dominant factor due to the pulse duration applied to the sciatic nerve (confinement region). However, as Wells et al. suggested [42], the heat diffusion begins immediately after the laser pulse and becomes considerably higher with pulses longer than 10 ms. Therefore, we assume that within the time duration of the stimulation pulse, there must be a thermal dissipation effect. Most of INS studies were conducted in the thermal confinement regime. However, Coventry et al. showed evidence of evoked CNAPs at 700-800 nm using very short pulses of 10 ns, i.e., in the regime of both thermal and stress confinement [77]. In this regard, neural activation may have different mechanisms at the cell membrane depending on whether the thermal or pressure confinement regime is prevailing.

The variability seen across experiments for the radiant exposure at stimulation threshold; and the sensitization effect can be explained by several factors. First, variation in heat absorption (during the stimulation pulse) and diffusion (within the time intervals between pulses of a stimulation train) based on the degree of hydration of the nerve, could lead to a higher efficiency of the stimulation, requiring lower power and shorter pulses for nerve excitation. Second, the presence or absence of connective tissue could decrease or increase the efficiency of INS. Third, variation in fiber stimulation optical thresholds. Fourth, the stimulating fiber core size and its positioning on the nerve have a significant influence, determining how spatial selective is optical stimulation. To illustrate this spatial selectivity, Figures 6 shows an electrical and optical recruitment curves in which the optical CNAP amplitude is about one order of magnitude lower than the electrical one. Whereas with electrical stimulation, the current spreads around the nerve volume, thus a bigger number of nerve fibers are recruited [36,42]; with optical stimulation, only the superficially located nerve fibers receiving the optical power will contribute to the CNAP. This amplitude difference of the CNAP between electrical and optical stimulation in our work (~ 90 %) are in line with the values reported in literature at 2120 nm (60-90 %) and 4000 nm (90 %) [36,44]. To explain this variation, we proposed three hypothesizes: 1) the level of hydration in the tissue (considering water as the main chromosphore in the energy transfer process); 2) the alignment of the optical fiber with the nerve fibers underneath could provide a better fit of energy deposition to the target; and 3) the variation of the thickness in the epineurium and perineurium in the rat sciatic nerve [85] might lead to a change in the amount

of energy deposited and thus in the volume of nerve fibers excited. Additionally, in Figure 6, the latency defined as the time from stimulus onset to the onset of the CNAP, also differs for optical and electrical stimulation. Hence, the type of excited nerve fibers differs when stimulating electrically or optically. If optically activated nerve fibers are relatively far from the recording electrodes, then no CNAP will be measured. This may support the fact that seven rats did not respond after an optical stimulus. For instance, in RAT 10, at the beginning of the recordings, no CNAPs were obtained, however, after moving the fiber to a slightly different position, CNAPs were recorded successfully. These results are in line with [58]. In this study, some locations of the rabbit sciatic nerve did not respond to optical stimulation while other sections were stimulated successfully. In two rats, we report evidence of simultaneous recordings of CNAPs with different conduction velocities. The slower conduction velocities recorded are in the range attributed to C fibres (i.e., in the range of 1 m/s). Our preliminary results therefore suggest that these fibres could be activated by optical stimuli. If confirmed, this finding would be of major importance. To explain why the later peaks were only observed in a low number of samples, we propose 3 hypotheses. First, the sciatic nerve is essentially a somatic nerve (containing somatosensory and somatomotor fibres, which are mostly A and in a small part C fibers). Therefore, the CNAP amplitude generated by these unmyelinated fibres in sciatic nerves is small. Second, the light spot size might have missed them. Third, the explored time window for stimulation might have been too short, leading to an energy deposition lower than the required for the activation of these small fibres. Vagus nerve would be a good candidate to study whether C fibres are best activated with optical stimulation, as it is a mixed nerve in contrast to others somatic nerves. It is essentially a visceral nerve with only a small somatic component (the visceral fibres are B and above all C type). Optical stimulation would open completely new clinical application fields considering that a nerve such as the vagus nerve contains mainly small unmyelinated fibres [109]. Future works will be conducted to analyse and implement stimulation of C fibres before fast fibres. Moreover, evaluating if the temperature diffusion matches Hodgkin–Huxley model for stimulation threshold vs. temperature, may give insights about stimulation efficiency at different power and pulse duration combinations.

CONFLICT OF INTEREST

The author confirms that this article has no conflict of interest.

ACKNOWLEDGEMENT

The research was supported by the Walloon Region, Belgium - Pôle Mecatech (Project NEUROPV n°7740).

REFERENCES

1. Merrill, D. R., Bikson, M., & Jefferys, J. G. (2005). Electrical stimulation of excitable tissue: design of efficacious and safe protocols. *Journal of neuroscience methods*, *141*(2), 171-198.
2. Krames, E. S., Peckham, P. H., Rezai, A., & Aboelsaad, F. (2009). What is neuromodulation? In *Neuromodulation* (pp. 3-8). Academic Press.
3. Vonck, K., De Herdt, V., Sprengers, M., & Ben-Menachem, E. (2012). Neurostimulation for epilepsy. In *Handbook of clinical neurology* (Vol. 108, pp. 955-970). Elsevier.
4. Wang, Y., Hutchings, F., & Kaiser, M. (2015). Computational modeling of neurostimulation in brain diseases. In *Progress in brain research* (Vol. 222, pp. 191-228). Elsevier.
5. Benchimol, A. (1966). Cardiac functions during electrical stimulation of the heart: Effect of exercise and drugs in patients with permanent pacemakers. *American Journal of Cardiology*, *17*(1), 27-42.
6. Obel, I. W., & Bourgeois, I. (1993). *U.S. Patent No. 5,199,428*. Washington, DC: U.S. Patent and Trademark Office.
7. Tchou, P. J., Kadri, N., Anderson, J., Caceres, J. A., Jazayeri, M., & Akhtar, M. (1988). Automatic implantable cardioverter defibrillators and survival of patients with left ventricular dysfunction and malignant ventricular arrhythmias. *Annals of Internal Medicine*, *109*(7), 529-534.
8. Troup, P. J. (1989). Implantable cardioverters and defibrillators. *Current problems in cardiology*, *14*(12), 673-815.
9. Deuschl, G., & Agid, Y. (2013). Subthalamic neurostimulation for Parkinson's disease with early fluctuations: balancing the risks and benefits. *The Lancet Neurology*, *12*(10), 1025-1034.
10. Reich, M. M., Steigerwald, F., Sawalhe, A. D., Reese, R., Gunalan, K., Johannes, S., ... & Volkmann, J. (2015). Short pulse width widens the therapeutic window of subthalamic neurostimulation. *Annals of clinical and translational neurology*, *2*(4), 427-432.
11. Fundament, T., Eldridge, P. R., Green, A. L., Whone, A. L., Taylor, R. S., Williams, A. C., & Schuepbach, W. M. (2016). Deep brain stimulation for Parkinson's disease with early motor complications: a UK cost-effectiveness analysis. *Plos one*, *11*(7), e0159340.
12. Herzog, J., Hamel, W., Wenzelburger, R., Pötter, M., Pinsker, M. O., Bartussek, J., ... & Volkmann, J. (2007). Kinematic analysis of thalamic versus subthalamic neurostimulation in postural and intention tremor. *Brain*, *130*(6), 1608-1625.
13. Groppa, S., Herzog, J., Falk, D., Riedel, C., Deuschl, G., & Volkmann, J. (2014). Physiological and anatomical decomposition of subthalamic neurostimulation effects in essential tremor. *Brain*, *137*(1), 109-121.
14. Jolly, C. N., Spelman, F. A., & Clopton, B. M. (1996). Quadrupolar stimulation for cochlear prostheses: modeling and experimental data. *IEEE transactions on biomedical engineering*, *43*(8), 857-865.
15. Schmidt, E. M., Bak, M. J., Hambrecht, F. T., Kufta, C. V., O'rourke, D. K., & Vallabhanath, P. (1996). Feasibility of a visual prosthesis for the blind based on intracortical micro stimulation of the visual cortex. *Brain*, *119*(2), 507-522.
16. Weese-Mayer, D. E. (1997). Diaphragm pacing by electrical stimulation of the phrenic nerve: 1996 update. *Pediatric Pulmonology*, *23*(2), 157-158.
17. Chervin, R. D., & Guilleminault, C. (1997). Diaphragm pacing for respiratory insufficiency. *Journal of clinical neurophysiology*, *14*(5), 369-377.
18. Tanagho, E. A., & Schmidt, R. A. (1988). Electrical stimulation in the clinical management of the neurogenic bladder. *The Journal of urology*, *140*(6), 1331-1339.
19. Chancellor, M. B., & Chartier-Kastler, E. J. (2000). Principles of sacral nerve stimulation (SNS) for the treatment of bladder and urethral sphincter dysfunctions. *Neuromodulation: Technology at the Neural Interface*, *3*(1), 16-26.
20. Kluding, P. M., Dunning, K., O'Dell, M. W., Wu, S. S., Ginosian, J., Feld, J., & McBride, K. (2013). Foot drop stimulation versus ankle foot orthosis after stroke: 30-week outcomes. *Stroke*, *44*(6), 1660-1669.
21. Dunning, K., O'Dell, M. W., Kluding, P., & McBride, K. (2015). Peroneal stimulation for foot drop after stroke: a systematic review. *American Journal of Physical Medicine & Rehabilitation*, *94*(8), 649-664.
22. Bajd, T., Kralj, A., Turk, R., Benko, H., & Šega, J. (1983). The use of a four-channel electrical stimulator as an ambulatory aid for paraplegic patients. *Physical Therapy*, *63*(7), 1116-1120.

23. Wieler, M., Stein, R. B., Ladouceur, M., Whittaker, M., Smith, A. W., Naaman, S., ... & Aimone, E. (1999). Multicenter evaluation of electrical stimulation systems for walking. *Archives of physical medicine and rehabilitation*, *80*(5), 495-500.
24. Zabara, J., Barrett, B. T., & Parnis, S. M. (2004). *U.S. Patent No. 6,721,603*. Washington, DC: U.S. Patent and Trademark Office.
25. Multon, S., & Schoenen, J. (2005). Pain control by vagus nerve stimulation: from animal to man... and back. *Acta neurologica belgica*, *105*(2), 62.
26. Chakravarthy, K., Chaudhry, H., Williams, K., & Christo, P. J. (2015). Review of the uses of vagal nerve stimulation in chronic pain management. *Current pain and headache reports*, *19*(12), 54.
27. Marangell, L. B., Martinez, M., Jurdi, R. A., & Zboyan, H. (2007). Neurostimulation therapies in depression: a review of new modalities. *Acta Psychiatrica Scandinavica*, *116*(3), 174-181.
28. De Raedt, R., Vanderhasselt, M. A., & Baeken, C. (2015). Neurostimulation as an intervention for treatment resistant depression: From research on mechanisms towards targeted neurocognitive strategies. *Clinical Psychology Review*, *41*, 61-69.
29. Val-Laillet, D., Biraben, A., Randuineau, G., & Malbert, C. H. (2010). Chronic vagus nerve stimulation decreased weight gain, food consumption and sweet craving in adult obese minipigs. *Appetite*, *55*(2), 245-252.
30. Mauskop, A. (2005). Vagus nerve stimulation relieves chronic refractory migraine and cluster headaches. *Cephalalgia*, *25*(2), 82-86.
31. Silberstein, S. D., Calhoun, A. H., Lipton, R. B., Grosberg, B. M., Cady, R. K., Dorlas, S., ... & Saper, J. R. (2016). Chronic migraine headache prevention with noninvasive vagus nerve stimulation: The EVENT study. *Neurology*, *87*(5), 529-538.
32. De Ferrari, G. M., Crijns, H. J., Borggrefe, M., Milasinovic, G., Smid, J., Zabel, M., ... & Raspopovic, S. (2011). Chronic vagus nerve stimulation: a new and promising therapeutic approach for chronic heart failure. *European heart journal*, *32*(7), 847-855.
33. Paulon, E., Nastou, D., Jaboli, F., Marin, J., Liebler, E., & Epstein, O. (2017). Proof of concept: short-term non-invasive cervical vagus nerve stimulation in patients with drug-refractory gastroparesis. *Frontline Gastroenterology*, *8*(4), 325-330.
34. Gottfried-Blackmore, A., Adler, E. P., Fernandez-Becker, N., Clarke, J., Habtezion, A., & Nguyen, L. (2020). Open-label pilot study: Non-invasive vagal nerve stimulation improves symptoms and gastric emptying in patients with idiopathic gastroparesis. *Neurogastroenterology & Motility*, *32*(4), e13769.
35. Dautrebande, M., Doguet, P., Gorza, S. P., Delbeke, J., Botquin, Y., & Nonclercq, A. (2016). In vivo photonic stimulation of sciatic nerve with a 1470 nm Laser. *European journal of translational myology*, *26*(3).
36. Wells, J., Kao, C., Mariappan, K., Albea, J., Jansen, E. D., Konrad, P., & Mahadevan-Jansen, A. (2005). Optical stimulation of neural tissue in vivo. *Optics letters*, *30*(5), 504-506.
37. Wininger, F. A., Schei, J. L., & Rector, D. M. (2009). Complete optical neurophysiology: toward optical stimulation and recording of neural tissue. *Applied optics*, *48*(10), D218-D224.
38. Dautrebande, M., Doguet, P., Gorza, S. P., Delbeke, J., & Nonclercq, A. (2018, February). Peripheral nerve recruitment curve using near-infrared stimulation. In *Optogenetics and Optical Manipulation 2018* (Vol. 10482, p. 104820V). International Society for Optics and Photonics.
39. Henneman, E. (1957). Relation between size of neurons and their susceptibility to discharge. *Science*, *126*(3287), 1345-1347.
40. Izzo, A. D., Richter, C. P., Jansen, E. D., & Walsh Jr, J. T. (2006). Laser stimulation of the auditory nerve. *Lasers in Surgery and Medicine: The Official Journal of the American Society for Laser Medicine and Surgery*, *38*(8), 745-753.
41. Teudt, I. U., Nevel, A. E., Izzo, A. D., Walsh Jr, J. T., & Richter, C. P. (2007). Optical stimulation of the facial nerve: a new monitoring technique? *The Laryngoscope*, *117*(9), 1641-1647.
42. Wells, J., Kao, C., Konrad, P., Milner, T., Kim, J., Mahadevan-Jansen, A., & Jansen, E. D. (2007). Biophysical mechanisms of transient optical stimulation of peripheral nerve. *Biophysical journal*, *93*(7), 2567-2580.
43. Wells, J. D., Thomsen, S., Whitaker, P., Jansen, E. D., Kao, C. C., Konrad, P. E., & Mahadevan-Jansen, A. (2007). Optically mediated nerve stimulation: Identification of injury thresholds. *Lasers in Surgery and Medicine: The Official Journal of the American Society for Laser Medicine and Surgery*, *39*(6), 513-526.
44. Wells, J., Konrad, P., Kao, C., Jansen, E. D., & Mahadevan-Jansen, A. (2007). Pulsed laser versus electrical energy for peripheral nerve stimulation. *Journal of neuroscience methods*, *163*(2), 326-337.
45. Izzo, A. D., Walsh, J. T., Jansen, E. D., Bendett, M., Webb, J., Ralph, H., & Richter, C. P. (2007). Optical parameter variability in laser nerve stimulation: a study of pulse duration, repetition rate, and wavelength. *IEEE Transactions on Biomedical Engineering*, *54*(6), 1108-1114.
46. Izzo, A. D., Walsh Jr, J. T., Ralph, H., Webb, J., Bendett, M., Wells, J., & Richter, C. P. (2008). Laser stimulation of auditory neurons: effect of shorter pulse duration and penetration depth. *Biophysical journal*, *94*(8), 3159-3166.
47. Richter, C. P., Bayon, R., Izzo, A. D., Otting, M., Suh, E., Goyal, S., ... & Walsh Jr, J. T. (2008). Optical stimulation of auditory neurons: effects of acute and chronic deafening. *Hearing research*, *242*(1-2), 42-51.
48. Fried, N. M., Lagoda, G. A., Scott, N. J., Su, L. M., & Burnett, A. L. (2008). Noncontact stimulation of the cavernous nerves in the rat prostate using a tunable-wavelength thulium fiber laser. *Journal of endourology*, *22*(3), 409-414.
49. Fried, N. M., Lagoda, G. A., Scott, N. J., Su, L. M., & Burnett, A. L. (2008, August). Laser stimulation of the cavernous nerves in the rat prostate, in vivo: optimization of wavelength, pulse energy, and pulse repetition rate. In *2008 30th Annual International Conference of the IEEE Engineering in Medicine and Biology Society* (pp. 2777-2780). IEEE.
50. Duke, A. R., Cayce, J. M., Malphrus, J. D., Konrad, P., Mahadevan-Jansen, A., & Jansen, E. D. (2009). Combined optical and electrical stimulation of neural tissue in vivo. *Journal of biomedical optics*, *14*(6), 060501.
51. McCaughey, R. G., Chlebicki, C., & Wong, B. J. (2010). Novel wavelengths for laser nerve stimulation. *Lasers in Surgery and Medicine: The Official Journal of the American Society for Laser Medicine and Surgery*, *42*(1), 69-75.
52. Littlefield, P. D., Vujanovic, I., Mundi, J., Matic, A. I., & Richter, C. P. (2010). Laser stimulation of single auditory nerve fibers. *The Laryngoscope*, *120*(10), 2071-2082.
53. Cayce, J. M., Friedman, R. M., Jansen, E. D., Mahavaden-Jansen, A., & Roe, A. W. (2011). Pulsed infrared light alters neural activity in rat somatosensory cortex in vivo. *Neuroimage*, *57*(1), 155-166.
54. Banakis, R. M., Matic, A. I., Rajguru, S. M., & Richter, C. P. (2011, February). Optical stimulation of the auditory nerve: effects of pulse shape. In *Photonic Therapeutics and Diagnostics VII* (Vol. 7883, p. 788358). International Society for Optics and Photonics.
55. Duke, A. R., Lu, H., Jenkins, M. W., Chiel, H. J., & Jansen, E. D. (2012). Spatial and temporal variability in response to hybrid electro-optical stimulation. *Journal of neural engineering*, *9*(3), 036003.
56. Duke, A. R., Peterson, E., Mackanos, M. A., Atkinson, J., Tyler, D., & Jansen, E. D. (2012). Hybrid electro-optical stimulation of the rat sciatic nerve induces force generation in the plantarflexor muscles. *Journal of neural engineering*, *9*(6), 066006.
57. Tozburun, S., Stahl, C. D., Hutchens, T. C., Lagoda, G. A., Burnett, A. L., & Fried, N. M. (2013). Continuous-wave infrared subsurface optical stimulation of the rat prostate cavernous nerves using a 1490-nm diode laser. *Urology*, *82*(4), 969-973.
58. Peterson, E. J., & Tyler, D. J. (2013). Motor neuron activation in peripheral nerves using infrared neural stimulation. *Journal of neural engineering*, *11*(1), 016001.

59. Cayce, J. M., Friedman, R. M., Chen, G., Jansen, E. D., Mahadevan-Jansen, A., & Roe, A. W. (2014). Infrared neural stimulation of primary visual cortex in non-human primates. *Neuroimage*, *84*, 181-190.
60. Cayce, J. M., Wells, J. D., Malphrus, J. D., Kao, C., Thomsen, S., Tulipan, N. B., ... & Mahadevan-Jansen, A. (2015). Infrared neural stimulation of human spinal nerve roots in vivo. *Neurophotonics*, *2*(1), 015007.
61. Guan, T., Zhu, K., Wang, J., Chen, F., He, Y., Wu, M., & Nie, G. (2015). Auditory nerve impulses induced by 980 nm laser. *Journal of biomedical optics*, *20*(8), 088004.
62. Throckmorton, G., Adams, W. R., Ricks, Z., Cayce, J., Jansen, E. D., & Mahadevan-Jansen, A. (2019, March). Comparing the efficacy and safety of infrared neural stimulation at 1450 nm and 1875 nm (Conference Presentation). In *Optogenetics and Optical Manipulation 2019* (Vol. 10866, p. 108660G). International Society for Optics and Photonics.
63. C Thompson, A., R Stoddart, P., & Jansen, E. D. (2014). Optical stimulation of neurons. *Current molecular imaging*, *3*(2), 162-177.
64. Rhee, A. Y., Li, G., Wells, J., & Kao, J. P. (2008, March). Photostimulation of sensory neurons of the rat vagus nerve. In Optical Interactions with Tissue and Cells XIX (Vol. 6854, p. 68540E). International Society for Optics and Photonics.
65. Suh, E., Matic, A. I., Otting, M., Walsh Jr, J. T., & Richter, C. P. (2009, February). Optical stimulation in mice lacking the TRPV1 channel. In *Photons and Neurons* (Vol. 7180, p. 71800S). International Society for Optics and Photonics.
66. Albert, E. S., Bec, J. M., Desmadryl, G., Chekroud, K., Travo, C., Gaboyard, S., ... & Hamel, C. (2012). TRPV4 channels mediate the infrared laser-evoked response in sensory neurons. Journal of neurophysiology, 107(12), 3227-3234.
67. Shapiro, M. G., Homma, K., Villarreal, S., Richter, C. P., & Bezanilla, F. (2012). Infrared light excites cells by changing their electrical capacitance. *Nature communications*, *3*(1), 1-11.
68. Beier, H. T., Tolstykh, G. P., Musick, J. D., Thomas, R. J., & Ibey, B. L. (2014). Plasma membrane nanoporation as a possible mechanism behind infrared excitation of cells. Journal of neural engineering, 11(6), 066006.
69. Ichinose, T., & Lukasiewicz, P. D. (2007). Ambient light regulates sodium channel activity to dynamically control retinal signaling. *Journal of Neuroscience*, *27*(17), 4756-4764.
70. Jelínková, H., Kőhler, O., Miyagi, M., Koranda, P., Němec, M., Šulc, J., ... & Matsuura, Y. (2009, February). Comparison of Ho: YAG and Er: YAG lasers for lithotripsy. In *Photonic Therapeutics.*
71. Jacques, S. L. (2013). Optical properties of biological tissues: a review. Physics in Medicine & Biology, 58(11), R37.
72. Highton, D., Tachtsidis, I., Tucker, A., Elwell, C., & Smith, M. (2016). Near infrared light scattering changes following acute brain injury. In Oxygen Transport to Tissue XXXVII (pp. 139-144). Springer, New York, NY.
73. Pu, Y., Chen, J., Wang, W., & Alfano, R. R. (2019). Basic optical scattering parameter of the brain and prostate tissues in the spectral range of 400–2400 nm. In Neurophotonics and Biomedical Spectroscopy (pp. 229-252). Elsevier.
74. Upputuri, P. K., & Pramanik, M. (2019). Photoacoustic imaging in the second near-infrared window: a review. Journal of biomedical optics, 24(4), 040901.
75. Jacques, S. L., & Pogue, B. W. (2008). Tutorial on diffuse light transport. Journal of biomedical optics, 13(4), 041302.
76. Jenkins, M. W., Duke, A. R., Gu, S., Doughman, Y., Chiel, H. J., Fujioka, H., ... & Rollins, A. M. (2010). Optical pacing of the embryonic heart. *Nature photonics*, *4*(9), 623-626.
77. Coventry, B. S., Sick, J. T., Talavage, T. M., Stantz, K. M., & Bartlett, E. L. (2020, July). Short-wave Infrared Neural Stimulation Drives Graded Sciatic Nerve Activation Across A Continuum of Wavelengths. In 2020 42nd Annual International Conference of the IEEE Engineering in Medicine & Biology Society (EMBC) (pp. 3581-3585). IEEE.
78. Jenkins, M. W., Wang, Y. T., Doughman, Y. Q., Watanabe, M., Cheng, Y., & Rollins, A. M. (2013). Optical pacing of the adult rabbit heart. *Biomedical optics express*, *4*(9), 1626-1635.
79. You, M., Zhou, R., & Mou, Z. (2019). Selective stimulation of bullfrog sciatic nerve by gold nanorod assisted combined electrical and near-infrared stimulation. *Biomedical microdevices*, *21*(3), 76.
80. Cargill, R., Baumann, T., & Jacques, S. L. (2008, February). Optical stimulation of excised murine sciatic nerve using 1.8-um wavelength laser. In *Optical Interactions with Tissue and Cells XIX* (Vol. 6854, p. 68540I). International Society for Optics and Photonics.
81. Kong, F., Jiao, R., Liu, K., Han, X., & Sun, C. (2019, November). Continuous infrared laser irradiation decreased membrane capacitance of neuron cell. In *Optics in Health Care and Biomedical Optics IX* (Vol. 11190, p. 111901X). International Society for Optics and Photonics.
82. Liljemalm, R., Nyberg, T., & von Holst, H. (2013). Heating during infrared neural stimulation. *Lasers in surgery and medicine*, *45*(7), 469-481.
83. Moallemi, P., & Behnampourii, M. (2010). Adaptive optimum notch filter for periodic noise reduction in digital images. AUT Journal of Electrical Engineering, 42(1), 1-7.
84. Jacques, S. L. (1992). Laser-tissue interactions. Photochemical, photothermal, and photomechanical. *The Surgical clinics of North America*, *72*(3), 531-558.
85. Hope, J., Braeuer, B., Amirapu, S., McDaid, A., & Vanholsbeeck, F. (2018). Extracting morphometric information from rat sciatic nerve using optical coherence tomography. Journal of biomedical optics, 23(11), 116001.
86. Luan, S., Williams, I., Nikolic, K., & Constandinou, T. G. (2014). Neuromodulation: present and emerging methods. Frontiers in neuroengineering, 7, 27
87. Loeb, G. E. (2018). Neural prosthetics: a review of empirical vs. systems engineering strategies. Applied Bionics and Biomechanics, 2018.
88. Spencer, T. C., Fallon, J. B., Thien, P. C., & Shivdasani, M. N. (2016). Spatial restriction of neural activation using focused multipolar stimulation with a retinal prosthesis. Investigative Ophthalmology & Visual Science, 57(7), 3181-3191.
89. Richardson, R. T., Ibbotson, M. R., Thompson, A. C., Wise, A. K., & Fallon, J. B. (2020). Optical stimulation of neural tissue. Healthcare Technology Letters, 7(3), 58-65.
90. Cogan, S. F., Ludwig, K. A., Welle, C. G., & Takmakov, P. (2016). Tissue damage thresholds during therapeutic electrical stimulation. Journal of neural engineering, 13(2), 021001.
91. Zhao, K., Tan, X., Young, H., & Richter, C. P. (2016). Stimulation of neurons with infrared radiation. In Biomedical Optics in Otorhinolaryngology (pp. 253-284). Springer, New York, NY.
92. Kou, L., Labrie, D., & Chylek, P. (1993). Refractive indices of water and ice in the 0.65-to 2.5-μm spectral range. Applied optics, 32(19), 3531-3540.
93. Hale, G. M., & Querry, M. R. (1973). Optical constants of water in the 200-nm to 200-μm wavelength region. Applied optics, 12(3), 555-563.
94. Palmer, K. F., & Williams, D. (1974). Optical properties of water in the near infrared. JOSA, 64(8), 1107-1110.
95. Anderson, R. R., Farinelli, W., Laubach, H., Manstein, D., Yaroslavsky, A. N., Gubeli III, J., ... & Williams, G. P. (2006). Selective photothermolysis of lipid-rich tissues: A free electron laser study. Lasers in Surgery and Medicine: The Official Journal of the American Society for Laser Medicine and Surgery, 38(10), 913-919.
96. Altman, K. W., & Plonsey, R. (1989). Analysis of the longitudinal and radial resistivity measurements of the nerve trunk. Annals of biomedical engineering, 17(4), 313-324.
97. Rozman, J., Pečlin, P., Ribarič, S., Godec, M., & Burja, J. (2018). An improved method of crafting a multi-electrode spiral cuff for the selective stimulation of peripheral nerves. Scientific reports, 8(1), 1-11

98. Lamas, J. A., Rueda-Ruzafa, L., & Herrera-Pérez, S. (2019). Ion Channels and Thermosensitivity: TRP, TREK, or Both? International Journal of Molecular Sciences, 20(10), 2371,
99. Cesare, P., Moriondo, A., Vellani, V., & McNaughton, P. A. (1999). Ion channels gated by heat. Proceedings of the National Academy of Sciences, 96(14), 7658-7663.
100. Wei, S. Q., Tao, Z. Y., Xue, Y., & Cao, D. Y. (2019). Peripheral Sensitization. In Peripheral Nerves-Injuries, Disorders and Treatment. IntechOpen.
101. Gangadharan, V., & Kuner, R. (2013). Pain hypersensitivity mechanisms at a glance. Disease models & mechanisms, 6(4), 889-895.
102. Sterratt, D. C. (2014). Q10: The Effect of Temperature on Ion Channel Kinetics.
103. Hille, B. (2001). Ion channels of excitable membranes (Sinauer, Sunderland, MA).
104. You, M., & Mou, Z. (2017). Model study of combined electrical and near-infrared neural stimulation on the bullfrog sciatic nerve. Lasers in medical science, 32(5), 1163-1172
105. Simanovskii, D. M., Mackanos, M. A., Irani, A. R., O'Connell-Rodwell, C. E., Contag, C. H., Schwettman, H. A., & Palanker, D. V. (2006). Cellular tolerance to pulsed hyperthermia. Physical Review E, 74(1), 011915
106. Lapicque, L. (1909). Definition experimentale de l'excitabilite. Soc Biol, 77, 280-283.
107. Blair, H. A. (1932). On the intensity-time relations for stimulation by electric currents. I. The Journal of general physiology, 15(6), 709-729.
108. Boinagrov, D., Loudin, J., & Palanker, D. (2010). Strength–duration relationship for extracellular neural stimulation: numerical and analytical models. Journal of neurophysiology, 104(4), 2236-2248.
109. Koo, B., Ham, S. D., Sood, S., & Tarver, B. (2001). Human vagus nerve electrophysiology: a guide to vagus nerve stimulation parameters. Journal of clinical neurophysiology, 18(5), 429-433.